Article

*Discovery Medicine* 2026; 38(212): 3002–3015
https://doi.org/10.24976/Discov.Med.202638212.231

# Norepinephrine Induces Inflammation- and Injury-Related Changes in Epicardial Adipose-Derived Cells via the p38 MAPK and NF-κB Signaling Pathways and Is Associated With Calcium-Handling Protein Changes and Cellular Injury in H9c2 Cells Exposed to Epicardial Adipose-Derived Cell Culture Media

Fu Li[1], Ping Chen[1], Lina Ma[1], Yu Wang[1], Shaojing Xi[1,*]

[1]Department of Cardiology, People's Hospital of Ningxia Hui Autonomous Region, Ningxia Medical University, 750002 Yinchuan, Ningxia Hui Autonomous Region, China
*Correspondence: xishaojing0318@163.com (Shaojing Xi)
Submitted: 9 July 2026 Revised: 31 July 2026 Accepted: 21 August 2026 Published: 23 September 2026

**Background: Norepinephrine may induce inflammatory changes and cellular injury in epicardial adipose-derived cells. This study investigated the effects of norepinephrine on these cells and examined calcium-related responses and cellular injury in H9c2 cells following exposure to media collected from differently treated epicardial adipose-derived cell cultures.**
**Methods: Adipogenically differentiated epicardial adipose-derived cells were treated with norepinephrine, atropine, or their combination. Inflammatory responses, apoptosis, autophagy-related protein expression, and activation of the p38 MAPK and NF-κB signaling pathways were evaluated using ELISA, flow cytometry, immunofluorescence, and Western blotting. H9c2 rat cardiomyoblasts were exposed to the corresponding culture media, designated as epicardial adipose tissue (EAT)-CM, norepinephrine (NE)-CM, atropine-CM, and NE + atropine-CM. Fluo-4 fluorescence intensity, calcium-handling protein expression, Cx43 expression, and apoptosis were assessed. Pathway inhibitors were used to investigate the roles of p38 MAPK and NF-κB signaling pathways in NE-induced inflammatory responses and cellular injury in epicardial adipose-derived cells.**
**Results: Compared with the control group, norepinephrine significantly increased Tumor necrosis factor-alpha (TNF-α), Interleukin-6 (IL-6), and leptin levels, decreased adiponectin levels, and promoted apoptosis and altered autophagy-related protein expression in epicardial adipose-derived cells (all $p < 0.05$). Norepinephrine also activated the p38 MAPK and NF-κB signaling pathways (all $p < 0.05$). Compared with the EAT-CM group, the NE-CM group showed increased Fluo-4 fluorescence intensity, reduced SERCA2a expression and PLB phosphorylation, enhanced RyR2 phosphorylation, decreased Cx43 expression, and increased apoptosis. These alterations were most pronounced in the NE + atropine-CM group. Treatment with SB203580 or Bay 11-7082 attenuated norepinephrine-induced inflammatory responses and cellular injury (all $p < 0.05$).**
**Conclusions: Norepinephrine activated the p38 MAPK and NF-κB signaling pathways and induced inflammatory changes and cellular injury in epicardial adipose-derived cells. H9c2 cells in the NE-CM and NE + atropine-CM groups showed coordinated changes in Fluo-4 fluorescence intensity, calcium-handling protein and Cx43 expression, and apoptosis. H9c2 cells exposed to media collected from norepinephrine-treated epicardial adipose-derived cell cultures showed calcium-related alterations and cellular injury.**

**Keywords:** norepinephrine; epicardial adipose-derived cells; H9c2 cells; calcium-handling proteins; p38 MAPK; NF-κB

## Introduction

Atrial fibrillation is highly prevalent in clinical practice and represents the most common type of sustained arrhythmia. It not only predisposes patients to serious complications such as stroke and heart failure, but also significantly increases mortality [1]. Recent studies have gradually revealed that epicardial adipose tissue (EAT), located on the surface of the myocardium, is not merely fat tissue used for lipid storage. Instead, it exhibits high metabolic activity and may participate in the entire process of atrial fibrillation, from disease onset to disease progression [2,3]. In addition, there is no fascial barrier between EAT and the myocardium. Therefore, various bioactive substances secreted by EAT can directly affect the myocardium through paracrine and vasocrine pathways, thereby altering myocardial structure and normal physiological function [4].

Under normal physiological conditions, EAT mainly secretes anti-inflammatory substances, such as adiponectin, to protect the heart [5]. However, under pathological condi-

tions, EAT undergoes phenotypic transformation. Among the overall changes in the indicators, the most prominent was the substantial release of inflammatory factors. The secretion of pro-inflammatory substances, such as Tumor necrosis factor-alpha (TNF-α) and Interleukin-6 (IL-6), is markedly increased, whereas adiponectin, which has anti-inflammatory effects, continues to decrease, gradually forming a chronic local inflammatory microenvironment [6]. The inflammation-induced remodeling process can lead to both structural and electrical remodeling of the atria, thereby promoting the onset and persistence of atrial fibrillation [7].

Autonomic nervous system imbalance, particularly enhanced sympathetic activity, is an important trigger for atrial fibrillation [8,9]. Norepinephrine (NE), the primary neurotransmitter of the sympathetic nervous system, regulates adipose tissue metabolism, inflammatory responses, and cell survival [10]. However, the underlying mechanisms by which sympathetic activation influences EAT function and its indirect effects on cardiomyocytes remain unclear.

At the molecular level, the p38 MAPK and NF-κB signaling pathways are key regulators of inflammatory responses and cellular stress [11,12]. Activation of the NF-κB pathway is typically characterized by p65 phosphorylation and nuclear translocation, accompanied by IκBα degradation, thereby promoting the transcription of inflammatory genes. Although these pathways play key roles in inflammation, their involvement in NE-induced inflammatory changes and cellular injury in epicardial adipocytes remains unclear.

Disruption of intracellular $Ca^{2+}$ homeostasis is one of the key mechanisms underlying cardiomyocyte dysfunction and arrhythmogenesis [13]. Abnormal expression or phosphorylation of calcium-handling proteins, such as SERCA2a, phospholamban (PLB), and ryanodine receptor 2 (RyR2), can impair calcium cycling, thereby increasing the risk of arrhythmias [14]. A previous study has linked adipocyte-derived mediators to calcium-related responses in cardiac-derived cells [15]. However, the relationship between sympathetic stimulation of epicardial adipocytes and calcium-related changes in H9c2 cells remains unclear.

Therefore, this study aimed to investigate norepinephrine-induced inflammation, apoptosis, and cellular injury in epicardial adipose-derived cells and to elucidate the involvement of the p38 MAPK and NF-κB signaling pathways. We further evaluated intracellular $Ca^{2+}$ levels, calcium-handling protein and Cx43 expression, and apoptosis in H9c2 cells following exposure to media derived from differently treated epicardial adipose-derived cell cultures. This study provides *in vitro* evidence supporting a relationship between norepinephrine-induced changes in epicardial adipose-derived cells and injury-related alterations in H9c2 cells.

## Materials and Methods

### *Specific Procedures for the Isolation and Culture of Epicardial Adipose-Derived Cells*

This animal experiment was approved by the Ethics Committee of the People's Hospital of Ningxia Hui Autonomous Region (Approval No. 2026-LL-228). Six 7-week-old male Sprague–Dawley (SD) rats weighing 180–260 g were purchased from Beijing Vital River Laboratory Animal Technology Co., Ltd. Tissues from individual rats were isolated and cultured separately without pooling, and each rat therefore represented an independent biological replicate. Before tissue collection, the rats were anesthetized with sodium pentobarbital (50 mg/kg, intraperitoneally). After deep anesthesia was confirmed by the absence of the pedal withdrawal reflex, the rats were euthanized by an additional intraperitoneal injection of sodium pentobarbital at an overdose of 150 mg/kg (20 mg/mL). Death was confirmed by the absence of spontaneous respiration, heartbeat, and pedal withdrawal reflex. The thoracic cavity was then opened immediately, the heart was removed, and epicardial adipose tissue from the dorsal atrioventricular groove was dissected under sterile conditions and transferred separately into ice-cold PBS for subsequent processing. Freshly isolated adipose tissue was repeatedly washed with phosphate-buffered saline (PBS; T494526, Shanghai Aladdin Biochemical Technology Co., Ltd., Shanghai, China) to remove residual blood from the tissue surface. The adipose tissue was then finely minced into small pieces and placed in a prepared 0.1% type I collagenase solution (COLA-10001, Cyagen Biosciences Inc., Guangzhou, China). After the tissue had been fully digested, the digestion reaction was terminated. The digested mixture was passed through a 70-μm cell strainer (352350, Corning Inc., Corning, NY, USA) to remove undigested tissue debris. The upper liquid was discarded, and the cells precipitated at the bottom of the tube were the stromal vascular fraction (SVF) cells. The cells were gently resuspended in culture medium, seeded into culture dishes, and cultured in an incubator. The cells were cultured in DMEM/F12 medium supplemented with 10% fetal bovine serum. During the experiment, cell growth and morphological characteristics were observed under an Olympus CKX53 inverted microscope (Tokyo, Japan). Representative fields were photographed to evaluate adipogenic differentiation. In addition, all primary cells intended for subsequent experiments were screened for mycoplasma contamination in advance, and no mycoplasma contamination was detected in any sample.

### *Adipogenic Induction and Differentiation*

When the cells in the culture dishes reached 80%–90% confluence, the original culture medium was replaced with adipogenic induction medium to initiate adipogenic differentiation. After the cells had been cultured in the induction

medium for 2–3 days, the medium was replaced with maintenance medium containing insulin only. Fresh medium was then replaced every 2–3 days. The entire differentiation induction process lasted approximately 7–10 days. The cells were continuously observed under a microscope. When abundant intracellular lipid droplets were observed, the cells were considered to have undergone adipogenic differentiation and were used for subsequent experiments.

### *Grouping and Drug Treatment of Adipogenically Differentiated Cells*

#### Dose-gradient Experiment

The cells were divided into three groups to evaluate the effects of different concentrations: the control group received no norepinephrine (NE, 0 μM), the low-dose NE group received 1 μM NE, and the high-dose NE group received 10 μM NE. All groups were treated continuously for 48 h.

#### Exploratory Norepinephrine and Atropine Treatment Experiment

Atropine was included as an exploratory pharmacological treatment rather than as a model of parasympathetic inhibition or autonomic imbalance. Four groups were established for comparison: the blank control group, the NE treatment group (10 μM; HY-13715, MedChemExpress, NJ, USA), the atropine treatment group (1 μM; HY-B1205, MedChemExpress, NJ, USA), and the NE + atropine combined treatment group (10 μM NE and 1 μM atropine). The treatment duration was 48 h for all four groups.

#### Signaling Pathway Inhibition Experiment

To verify the roles of the p38 mitogen-activated protein kinase (p38 MAPK) and nuclear factor kappa B (NF-κB) signaling pathways, four groups were established: the blank control group, the NE treatment group (10 μM), the NE + SB203580 group (SB203580, 5 μM; EY-19875, Shanghai Yiyan Bio-technology Co., Ltd., Shanghai, China), and the NE + Bay 11-7082 group (Bay 11-7082, 5 μM; LM1523, Shanghai Lianmai Bioengineering Co., Ltd., Shanghai, China).

For the inhibitor-treated groups, cells were pretreated with SB203580 or Bay 11-7082 for 1 h, followed by NE stimulation for an additional 48 h.

### *Preparation of Culture Supernatants From Epicardial Adipose-Derived Cells and H9c2 Cell Treatment*

Adipogenically differentiated epicardial adipose-derived cells were treated according to the predefined groups for 48 h. After treatment, the culture medium was removed, and the cells were washed three times with PBS and incubated in serum-free DMEM/F12 for an additional 24 h to collect the conditioned medium. The collected supernatants were centrifuged at low temperature to remove cells and cellular debris and then concentrated using a 3-kDa molecular-weight-cutoff ultrafiltration device (UFC900396, Merck Millipore, Burlington, MA, USA). The concentrated samples were adjusted to the same total protein concentration with serum-free medium before subsequent H9c2 cell treatment. It should be noted that the samples in this experiment were not normalized according to the number of viable donor cells.

H9c2(2-1) rat cardiomyoblasts (CL-0089, Procell Life Science & Technology Co., Ltd., Wuhan, China) were routinely cultured and passaged. The cell line was authenticated by short tandem repeat (STR) profiling by the supplier, and the cells were confirmed to be free of mycoplasma contamination before use. Five treatment groups were established. The basal group was maintained in standard growth medium and was included only as a reference for the basal state of H9c2 cells. The EAT-CM group received conditioned medium collected from untreated epicardial adipose-derived cell cultures and served as the primary control for comparisons among the conditioned-medium groups. The NE-CM, atropine-CM, and NE + atropine-CM groups received conditioned media collected from epicardial adipose-derived cell cultures treated with 10 μM NE, 1 μM atropine, or their combination, respectively. H9c2 cells were exposed to the corresponding media for 48 h before subsequent assessments.

### *Oil Red O Staining*

Before staining, the old culture medium was completely removed from the culture wells. The adherent cells were then gently washed twice with PBS to thoroughly remove the remaining medium and avoid interference with subsequent staining. After washing, 4% paraformaldehyde fixative (KGIHC016, Jiangsu KeyGEN BioTECH Corp., Ltd., Nanjing, China) was added to preserve cell morphology and stabilize cellular structures, thereby preventing cell damage or detachment during staining. After fixation, the fixative was removed, and the cells were briefly washed once with PBS. Freshly prepared Oil Red O working solution (O0625, Sigma-Aldrich, St. Louis, MO, USA) was then added, and the cells were stained at room temperature to visualize intracellular lipid droplets. After staining, the excess staining solution was removed, and the cells were repeatedly and gently washed with distilled water to remove unbound free dye until the background appeared clear and no excess red staining remained. Finally, intracellular lipid droplet staining was observed under an inverted microscope at 200× magnification, and multiple representative fields were randomly selected for imaging. To ensure comparability among groups and reduce experimental error, the illumination intensity, white balance, and camera settings were kept consistent across all groups during image acquisition. Oil Red O-stained images were quantitatively analyzed using ImageJ software (version 1.54t, National Institutes of Health, Bethesda, MD, USA). Five randomly se-

lected, non-overlapping fields were analyzed for each sample. The mean staining intensity was measured using uniform analysis settings for all images within the same experimental batch. The mean value of the control group was set to 1, and the results were expressed as relative staining intensity.

### *Immunofluorescence*

Sterilized coverslips were placed in 24-well plates in advance, and the cells were then seeded. Subsequent drug treatments were performed when the cells reached an appropriate growth state. After all drug treatments were completed, the culture medium was removed, and the cells were washed three times with PBS. The cells were then fixed with 4% paraformaldehyde to preserve cellular morphology and prevent damage to cellular structures during subsequent procedures. After fixation, the solution was removed, and the cells were treated with 0.1% Triton X-100 (XY-0096, XY-Bioscience, Shanghai, China) to permeabilize the cell membrane, allowing antibodies to enter the cells and bind to the target proteins. After treatment, the cells were incubated at room temperature to block nonspecific binding sites and reduce nonspecific background fluorescence in subsequent images. Primary antibodies against PPARγ and Perilipin were used. The PPARγ primary antibody was diluted to 1:100 (sc-271392, Santa Cruz Biotechnology, Inc., Dallas, TX, USA), and the Perilipin primary antibody was diluted to 1:500 (PA1-1051, Thermo Fisher Scientific, Waltham, MA, USA). After addition of the primary antibodies, the cells were incubated overnight to ensure sufficient antigen–antibody binding. For pathway-related detection, a p65 primary antibody (6956, dilution 1:400, Cell Signaling Technology, Danvers, MA, USA) was used to observe the translocation of p65 into the nucleus. On the following day, the culture plates were removed from the refrigerator, and the primary antibody solutions were aspirated. The cells were thoroughly washed with PBS to remove unbound primary antibodies. For double-immunofluorescence staining, the corresponding fluorescent secondary antibodies were added as required. PPARγ was detected using an Alexa Fluor 488-conjugated goat anti-mouse IgG (H+L) secondary antibody (A-11029, dilution 1:1000, Invitrogen, Thermo Fisher Scientific, Waltham, MA, USA). Perilipin was detected using an Alexa Fluor 594-conjugated goat anti-rabbit IgG (H+L) secondary antibody (A-11037, dilution 1:1000, Invitrogen, Thermo Fisher Scientific, Waltham, MA, USA). The p65 staining group also received the Alexa Fluor 488-conjugated goat anti-mouse IgG (H+L) secondary antibody. All secondary antibodies were incubated for 1 h at room temperature in the dark. After incubation with secondary antibody, DAPI staining solution (D609734, Shanghai Aladdin Biochemical Technology Co., Ltd., Shanghai, China) was added to label the nuclei.

Fluorescence images were acquired using a BZ-X710 fluorescence microscope (Keyence Corporation) with a 40× objective. The imaging parameters for each fluorescence channel, including illumination intensity, exposure time, and gain, were first adjusted using the control group. Once established, the same settings were applied to all experimental groups. Areas with fluorescence overexposure were deliberately avoided during field selection to prevent data distortion. For analysis of the positive rates of adipogenic markers, five randomly selected, non-overlapping fields were examined for each sample. ImageJ software was used to count PPARγ-positive cells, Perilipin-positive cells, and all DAPI-stained nuclei. The positive rate of each marker was calculated by dividing the number of positive cells by the total number of nuclei and multiplying by 100%. A uniform fluorescence threshold was applied to all images from the same experimental batch. p65 nuclear translocation was quantitatively analyzed using ImageJ software. Five randomly selected, non-overlapping fields were analyzed for each sample. Nuclear regions were defined based on DAPI staining, and the mean fluorescence intensity of p65 within the nuclear region was measured. The same image-acquisition parameters and analysis thresholds were applied to all groups, and nuclear p65 fluorescence intensity was used to evaluate the extent of p65 nuclear translocation.

### *CCK-8 Assay*

Cell viability in each group was assessed using a Cell Counting Kit-8 (CCK-8; C266180, Shanghai Aladdin Biochemical Technology Co., Ltd., Shanghai, China), and all procedures were performed strictly according to the manufacturer's instructions. After all drug treatments were completed, 10 μL of CCK-8 solution was added to each well. The plate was gently shaken to ensure thorough mixing of the reagent with the culture medium and was then incubated at 37 °C. After the reaction, the OD value of each well was measured at 450 nm using a microplate reader, and the resulting data were used to assess cell viability in each group.

### *ELISA*

ELISA was used to assess the levels of inflammatory factors and adipokines in cell culture supernatants, and all procedures were performed strictly according to the instructions provided with the kits. Detection kits from different manufacturers were used. TNF-α levels were evaluated using an imported kit (RTA00, R&D Systems, Minneapolis, MN, USA). IL-6 (E-HSEL-R0004), adiponectin (E-EL-R3012), and leptin (E-EL-R0582) levels were measured using rat-specific ELISA kits from Elabscience Biotechnology Co., Ltd. (Wuhan, China). After drug treatment, the culture supernatants from each group were collected, transferred into centrifuge tubes, and centrifuged. The clear upper supernatants were collected for subsequent detection. After incubation, biotin-labeled detection antibodies were added, followed by further incubation. Horseradish perox-

idase (HRP)-labeled streptavidin was then added, and the samples were incubated again. After the plates were thoroughly washed, 3,3′,5,5′-tetramethylbenzidine (TMB) substrate was added for color development in the dark. When a uniform color gradient was observed in the standard wells, stop solution was immediately added to terminate the reaction. Finally, the absorbance of each well was measured at 450 nm using a microplate reader, and the values were used to calculate the concentrations of the factors in the samples and for subsequent data analysis.

### *Flow Cytometry*

Cell apoptosis was assessed using an Annexin V-FITC/PI double-staining apoptosis detection kit (HY-K1073, MedChemExpress, Monmouth Junction, NJ, USA), and all procedures were performed strictly according to the manufacturer's instructions. Cellular fluorescence signals were acquired using a BD FACSAria III flow cytometer, and the resulting data were analyzed using FlowJo software, version 10.8.1 (BD Life Sciences, Ashland, OR, USA). During data analysis, the valid cell population was first gated on the forward scatter area (FSC-A)/side scatter area (SSC-A) scatter plot to exclude cellular debris, impurity particles, and other invalid signals. Single cells were then selected based on FSC-H and FSC-A parameters to exclude cell aggregates and ensure detection accuracy. The total apoptosis rate was calculated as the sum of the percentages of early and late apoptotic cells. To ensure consistency and comparability among groups, identical flow cytometric gating parameters were applied to all samples without individual adjustment of thresholds or gating ranges.

### *Western Blotting*

Total cellular proteins were extracted using RIPA lysis buffer (U10001, Suzhou Yuyou Biotechnology Co., Ltd., Suzhou, China) supplemented with protease inhibitor (P665818, Shanghai Aladdin Biochemical Technology Co., Ltd., Shanghai, China) and phosphatase inhibitor (P777310, Shanghai Aladdin Biochemical Technology Co., Ltd., Shanghai, China) to prevent protein degradation and loss of phosphorylation signals. After lysis, the samples were centrifuged, and the clear upper protein supernatants were collected for subsequent experiments.

The proteins examined in this study and the corresponding primary antibodies were classified according to their functions as follows:

**Autophagy-related proteins:** microtubule-associated protein 1 light chain 3A/B (LC3A/B; 4108, dilution 1:1000, Cell Signaling Technology, Danvers, MA, USA) and p62/sequestosome 1 (p62/SQSTM1; 5114, dilution 1:1000, Cell Signaling Technology).

**Signaling pathway-related proteins:** phosphorylated p38 mitogen-activated protein kinase (Thr180/Tyr182, p-p38 MAPK; 4631, dilution 1:1000, Cell Signaling Technology), p38 mitogen-activated protein kinase (p38 MAPK; 8690, dilution 1:1000, Cell Signaling Technology), phosphorylated nuclear factor kappa B p65 (Ser536, p-NF-κB p65; 3033, dilution 1:1000, Cell Signaling Technology), nuclear factor kappa B p65 (NF-κB p65; 6956, dilution 1:1000, Cell Signaling Technology), and inhibitor of nuclear factor kappa B alpha (IκBα; 9242, dilution 1:1000, Cell Signaling Technology).

**Calcium-handling proteins:** sarcoplasmic/endoplasmic reticulum $Ca^{2+}$-ATPase 2a (SERCA2a; A010-20, dilution 1:5000, Badrilla Ltd., Leeds, UK), phosphorylated phospholamban (Ser16, p-phospholamban, p-PLB; A010-12AP, dilution 1:1000, Badrilla Ltd.), phospholamban (PLB; A010-14, dilution 1:5000, Badrilla Ltd.), phosphorylated ryanodine receptor 2 (Ser2808, p-ryanodine receptor 2, p-RyR2; A010-30AP, dilution 1:1000, Badrilla Ltd.), and ryanodine receptor 2 (RyR2; ab302716, dilution 1:1000, Abcam, Cambridge, UK).

**Other protein and loading control:** Connexin43 (3512, dilution 1:1000, Cell Signaling Technology) and glyceraldehyde-3-phosphate dehydrogenase (GAPDH; 5174, dilution 1:1000, Cell Signaling Technology).

After primary antibody incubation, the membranes were repeatedly washed with Tris-buffered saline containing Tween 20 (TBST; ZN2925, Beijing Baiaolaibo Technology Co., Ltd., Beijing, China) to remove unbound primary antibodies. According to the host species of the primary antibodies, the membranes were incubated with HRP-conjugated goat anti-rabbit IgG (SA00001-2, Proteintech, Wuhan, China; 1:5000) or HRP-conjugated goat anti-mouse IgG (SA00001-1, Proteintech, Wuhan, China; 1:5000) for 1 h at room temperature. After another thorough wash, protein signals were detected using an enhanced chemiluminescence (ECL) system, and images of the protein bands were captured (32209, Thermo Fisher Scientific, Waltham, MA, USA). Band intensities were measured using ImageJ software (version 1.54t, National Institutes of Health, Bethesda, MD, USA) for semi-quantitative analysis. The ratios of LC3-II to LC3-I, phosphorylated p38 to total p38, phosphorylated p65 to total p65, phosphorylated PLB to total PLB, and phosphorylated RyR2 to total RyR2 were calculated. The expression levels of all target proteins were normalized to GAPDH.

### *Fluo-4 AM Fluorescence Measurement*

Intracellular calcium fluorescence was detected using the Fluo-4 AM calcium-sensitive fluorescent probe (HY-101896, MedChemExpress, Monmouth Junction, NJ, USA). The cells were washed twice with serum-free culture medium. The prepared Fluo-4 AM working solution was then added for incubation to allow sufficient intracellular loading of the probe. After all procedures were completed, fluorescence images were acquired using a 20× objective to measure the intensity of the calcium fluorescence signal in each group. Within the same experiment, the excitation intensity, exposure time, gain, and other imaging parame-

ters were kept identical across all groups and remained unchanged throughout image acquisition. Five randomly selected, non-overlapping fields were analyzed for each sample. After background fluorescence was subtracted, the mean fluorescence intensity per cell was quantified using ImageJ software. The results were then compared with the mean value of the basal control group, which was set to 1, to calculate the relative fluorescence level of each group.

### *LDH Release Assay*

Cellular injury was assessed using an LDH Cytotoxicity Assay Kit (C0016, Beyotime Biotech Inc., Shanghai, China). After drug treatment, the samples were centrifuged, and the clear supernatants were retained for subsequent detection. An equal volume of LDH working reaction solution was added to each supernatant sample, followed by incubation. To accurately determine the maximum level of cellular injury, maximum-release control wells were separately established. All cells in these wells were completely lysed using the lysis solution supplied with the kit to release all intracellular LDH. This value was used as the reference for maximum LDH release and subsequent cytotoxicity calculation.

### *Statistical Analysis*

All statistical analyses were performed using GraphPad Prism software (version 9.0, GraphPad Software, Inc., San Diego, CA, USA). The Shapiro–Wilk test was used to assess whether the data in each group followed a normal distribution. All variables were normally distributed and are therefore presented as the mean ± standard deviation (SD). Differences between two groups were analyzed using an unpaired Student's *t*-test. For comparisons involving three or more groups, one-way analysis of variance (one-way ANOVA) was performed, followed by Tukey's multiple-comparison test for pairwise comparisons. All statistical tests were two-sided, and a $p$ value $< 0.05$ was considered statistically significant.

## Results

### *Isolation of Epicardial Adipose-derived Cells and Evaluation of Adipogenic Differentiation*

Epicardial adipose tissue was obtained from adult male Sprague–Dawley (SD) rats, and epicardial adipose-derived cells were subsequently isolated and subjected to adipogenic differentiation. Before induction, the cells mainly exhibited a spindle-shaped morphology. After 7–10 days of adipogenic induction, intracellular lipid droplet accumulation became evident, although some cells retained an elongated morphology (Fig. 1A,B). Immunofluorescence staining showed stronger PPARγ and Perilipin signals after differentiation. Quantitative analysis further showed that the percentages of PPARγ-positive and Perilipin-positive cells among DAPI-positive cells were significantly higher in the differentiated group than in the undifferentiated group (both $p < 0.001$) (Fig. 1C–F). These findings support successful adipogenic differentiation of the isolated epicardial adipose-derived cells.

### *Norepinephrine Induces Inflammation- and Injury-Related Changes in Epicardial Adipose-Derived Cells*

Oil Red O staining revealed a reduction in intracellular lipid accumulation following NE exposure. Lipid content was lower than that in the control group even at 1 μM NE ($p < 0.05$). When the concentration was increased to 10 μM, the lipid droplets became more fragmented, accompanied by a further decrease in total lipid accumulation ($p < 0.05$), as shown in Fig. 2A,B. After 48 h of treatment, the CCK-8 assay revealed only a slight decline in cell viability in the 1 μM group, whereas a more pronounced reduction occurred in the 10 μM group ($p < 0.05$), as shown in Fig. 2C.

NE exposure was also associated with changes in the extracellular levels of inflammatory mediators and adipokines. TNF-α and IL-6 concentrations increased at both tested doses, and the changes were greater after treatment with 10 μM NE. By contrast, adiponectin concentrations declined, whereas leptin concentrations increased ($p < 0.05$), as shown in Fig. 2D–G. These findings indicate that NE treatment was associated with changes in inflammatory mediator and adipokine levels in epicardial adipose-derived cell cultures.

Flow cytometric analysis identified a higher proportion of apoptotic cells following NE treatment. The increase was moderate at 1 μM but became more evident at 10 μM ($p < 0.05$). Both early and late apoptotic populations contributed to this change, as shown in Fig. 2H,I.

NE treatment also affected autophagy-related proteins. The LC3-II/LC3-I ratio increased, whereas p62 expression declined, with the largest changes observed in the 10 μM group ($p < 0.05$), as shown in Fig. 2J–L. These results indicate that NE treatment was associated with changes in autophagy-related protein expression in epicardial adipose-derived cells. However, autophagic flux was not directly assessed.

### *Effects of Norepinephrine and Atropine on Inflammatory Responses and p38 MAPK and NF-κB Pathway Activation in Epicardial Adipose-Derived Cells*

To clarify the effects of combined NE and atropine treatment on epicardial adipose-derived cells, cells were treated with NE, atropine, or their combination for 48 h. As shown in Fig. 3A–D, ELISA results showed that NE treatment increased TNF-α, IL-6, and leptin levels, while decreasing adiponectin levels ($p < 0.05$). In contrast, atropine alone produced only mild changes in these inflammation-related indicators. Among the four groups, the combined NE and atropine treatment group showed the most pro-

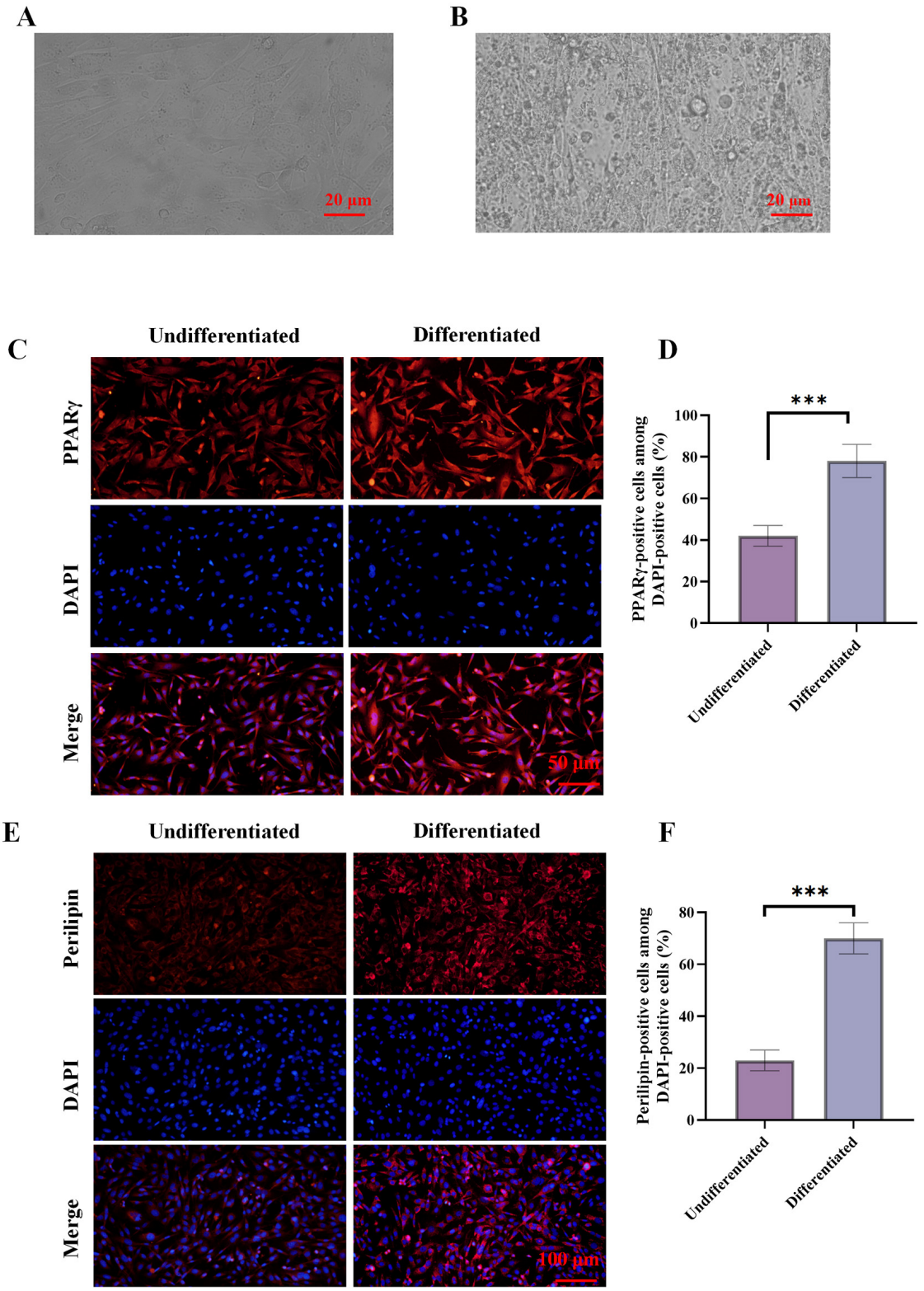


**Fig. 1. Morphological and phenotypic characterization of epicardial adipose-derived cells before and after adipogenic differentiation**. (A,B) Representative morphological images of epicardial adipose-derived cells before and after adipogenic differentiation, respectively. (C,D) Representative immunofluorescence images of PPARγ expression and the percentage of PPARγ-positive cells among DAPI-positive cells. (E,F) Representative immunofluorescence images of Perilipin expression and the percentage of Perilipin-positive cells among 4′,6-diamidino-2-phenylindole (DAPI)-positive cells. n = 6. ***$p < 0.001$.

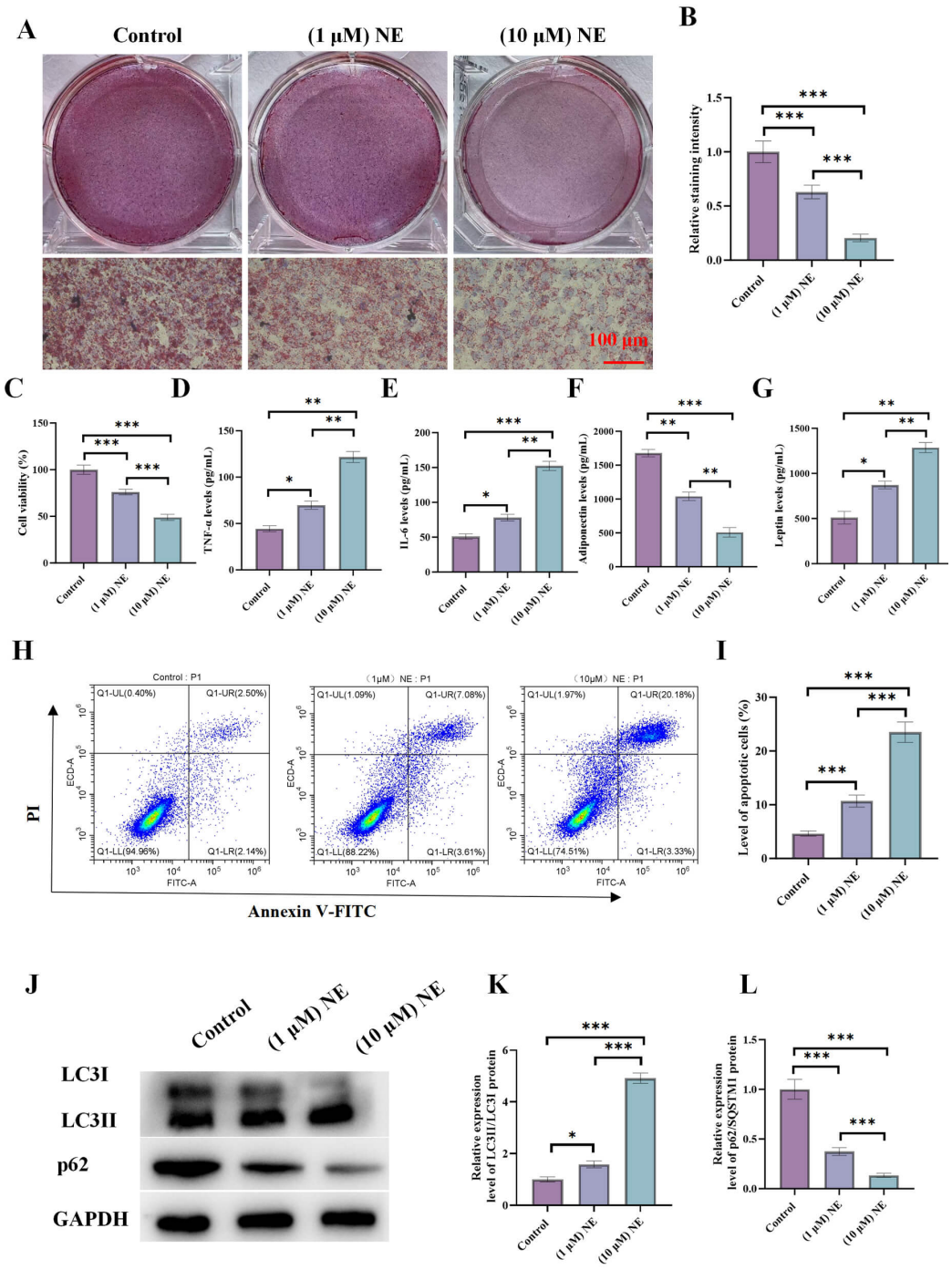


**Fig. 2. Norepinephrine induces inflammation- and injury-related changes, apoptosis, and autophagy-related protein changes in epicardial adipose-derived cells**. (A,B) Oil Red O staining was used to assess lipid accumulation in epicardial adipose-derived cells. (C) CCK-8 assay was used to evaluate changes in cell viability. (D–G) ELISA was used to measure Tumor necrosis factor-alpha (TNF-α), Interleukin-6 (IL-6), adiponectin, and leptin levels. (H,I) Cell apoptosis was assessed by Annexin V-fluorescein isothiocyanate/propidium iodide (Annexin V-FITC/PI) double-staining flow cytometry. (J–L) Western blot analysis and quantification of LC3-II/LC3-I and p62 expression. n = 6. *$p < 0.05$, **$p < 0.01$, and ***$p < 0.001$.

nounced changes ($p < 0.05$). Western blot analysis showed that NE activated the p38 MAPK and NF-κB signaling pathways. This was reflected by increases in the p-p38/p38 and p-p65/p65 ratios, together with enhanced IκBα degradation. The greatest changes were observed in the combined treatment group ($p < 0.05$), as shown in Fig. 3E–H. Immunofluorescence analysis further confirmed this trend. NE treatment increased the nuclear translocation of p65, and the

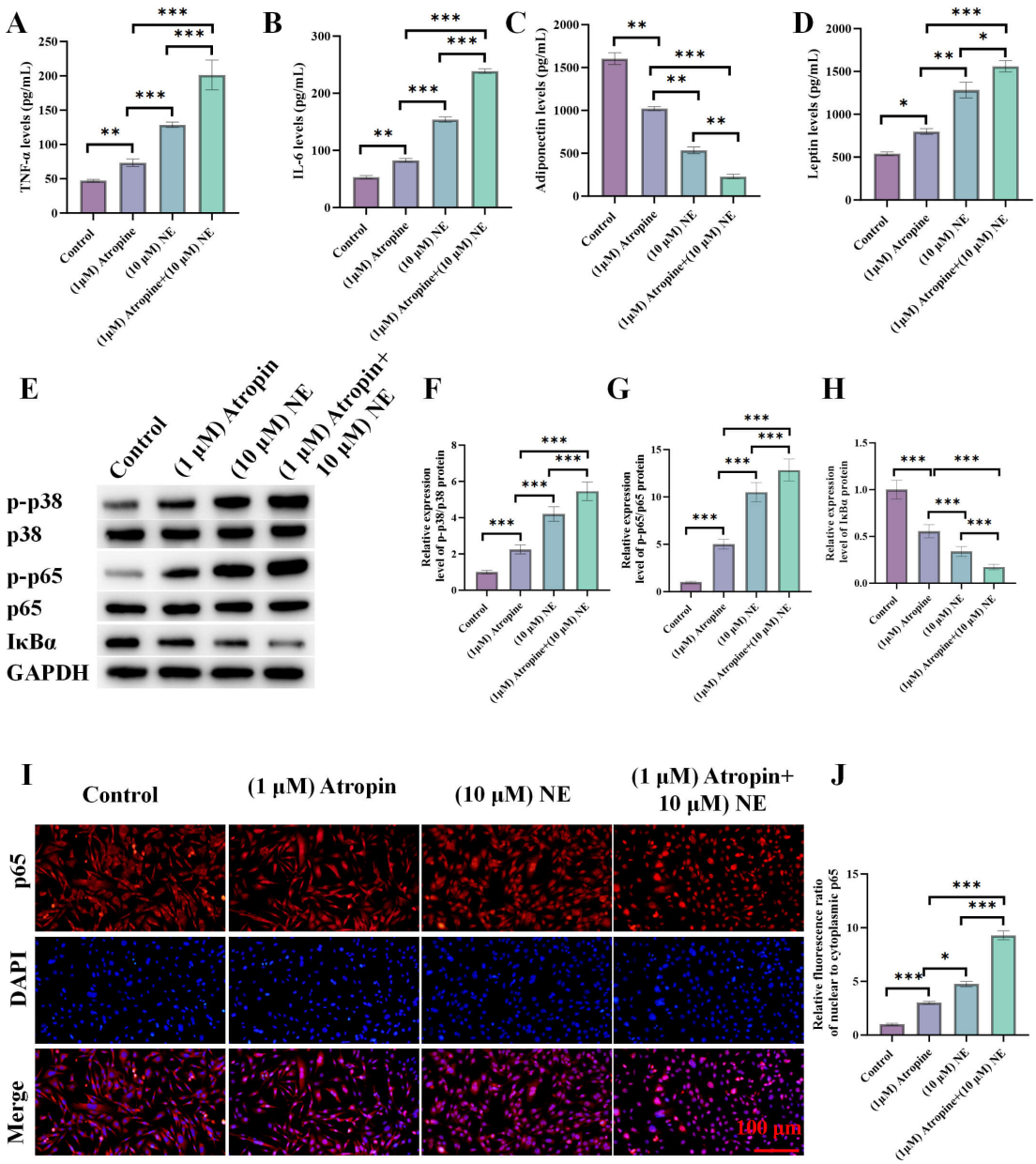


**Fig. 3. Effects of norepinephrine and atropine on inflammatory responses and p38 MAPK and NF-κB pathway activation in epicardial adipose-derived cells**. (A–D) ELISA showing TNF-α, IL-6, adiponectin, and leptin levels after NE, atropine, and combined treatments. (E–H) Western blot analysis of p38 MAPK and NF-κB pathway activation (p-p38/p38, p-p65/p65, and IκBα degradation). (I,J) Immunofluorescence showing nuclear translocation of p65. n = 6. *$p < 0.05$, **$p < 0.01$, and ***$p < 0.001$.

strongest nuclear p65 fluorescence signal was observed in the combined treatment group ($p < 0.05$), as shown in Fig. 3I,J.

### *Culture Supernatants Collected From Drug-Treated Epicardial Adipose-Derived Cell Cultures Were Associated With Changes in Intracellular $Ca^{2+}$ Levels, Calcium-Handling Protein Expression, and Apoptosis in H9c2 Cells*

Fluo-4 fluorescence intensity was markedly increased in the NE-CM and atropine-CM groups compared with the EAT-CM group, with the highest fluorescence intensity observed in the NE + atropine-CM group. All differences were statistically significant (all $p < 0.05$), as shown in Fig. 4A,B. Western blot analysis showed that SERCA2a expression and PLB phosphorylation were decreased, whereas RyR2 phosphorylation was increased, in the NE-CM and atropine-CM groups compared with the EAT-CM group. All differences were statistically significant (all $p < 0.05$), as shown in Fig. 4C–G. The greatest changes were observed in the NE + atropine-CM group ($p < 0.05$), indicating marked alterations in both the expression and phosphory-

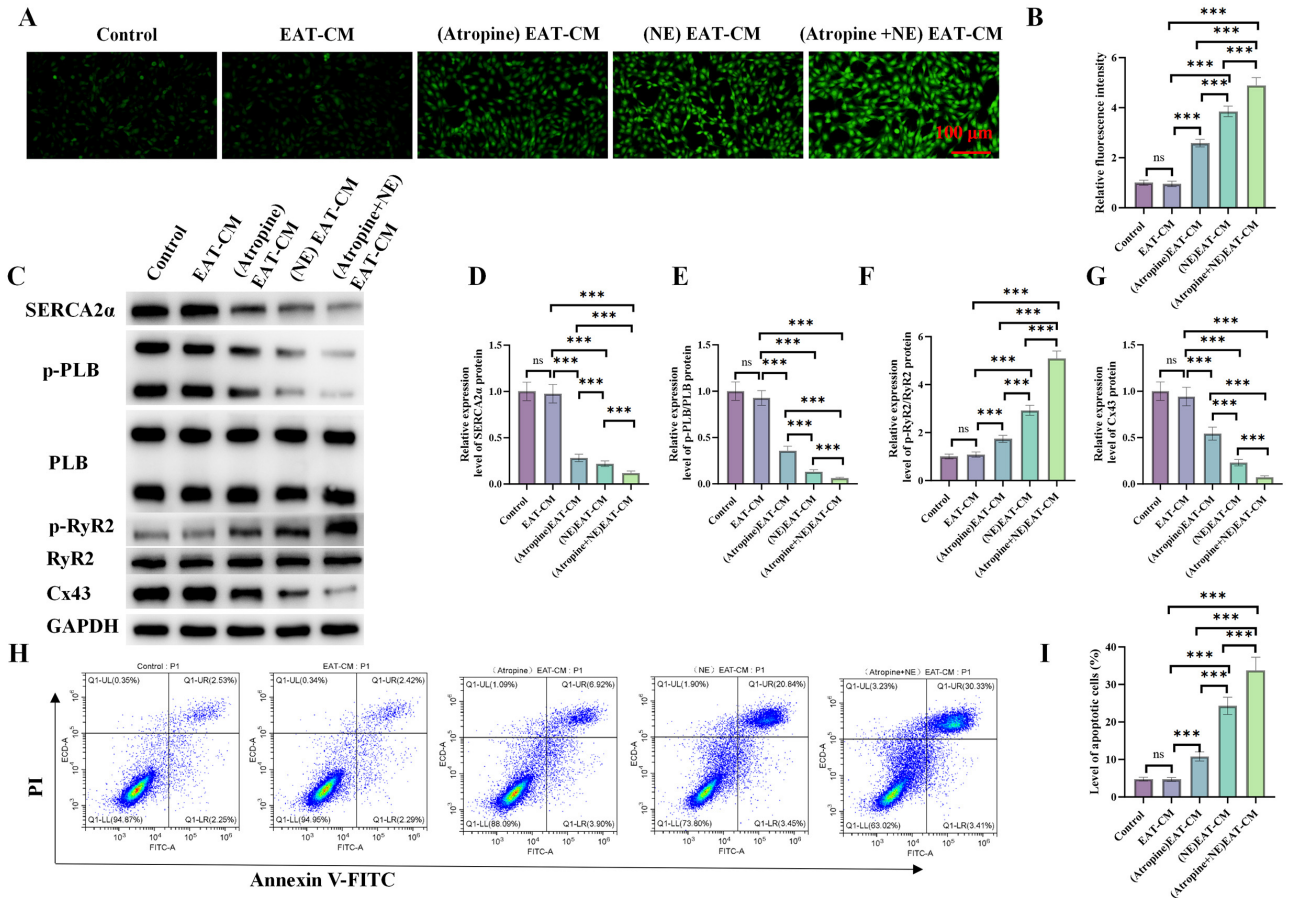


**Fig. 4. Culture supernatants collected from drug-treated epicardial adipose-derived cell cultures were associated with changes in intracellular $Ca^{2+}$ levels, calcium-handling protein expression, and apoptosis in H9c2 cells.** (A,B) Fluo-4 fluorescence intensity in H9c2 cells. (C–G) Western blot analysis of calcium-handling proteins, including SERCA2a, PLB and its phosphorylation, RyR2 and its phosphorylation, and Cx43 expression. (H,I) Flow cytometry analysis of H9c2 cell apoptosis. n = 6. ***$p < 0.001$.

lation of calcium-handling proteins in H9c2 cells. Cx43 expression was also lower in the NE-CM group than in the EAT-CM group ($p < 0.05$). Flow cytometric analysis showed that the apoptosis rates were higher in the NE-CM and atropine-CM groups than in the EAT-CM group ($p < 0.05$), with the highest apoptosis rate observed in the NE + atropine-CM group ($p < 0.05$), as shown in Fig. 4H,I. Overall, intracellular $Ca^{2+}$ levels, calcium-handling proteins, Cx43 expression, and apoptosis in H9c2 cells changed concurrently, showing a coordinated pattern of alterations.

### *p38 MAPK and NF-κB Are Involved in NE-Induced Inflammatory Responses and Cellular Injury in Epicardial Adipose-Derived Cells*

To clarify the roles of the p38 MAPK and NF-κB pathways in NE-induced inflammation and injury in epicardial adipose-derived cells, pathway-blocking experiments were performed using SB203580 and Bay 11-7082, respectively. As shown in Fig. 5A–D, compared with the control group, NE treatment markedly increased the phosphorylation levels of p38 and p65 and enhanced IκBα degradation ($p < 0.05$). Compared with the NE group, the NE + SB203580 group showed lower p-p38/p38 and p-p65/p65 ratios ($p < 0.05$). Bay 11-7082 also suppressed p65 phosphorylation and reduced IκBα degradation. It additionally decreased p38 phosphorylation, although this effect was weaker than that observed with SB203580. All differences were statistically significant (all $p < 0.05$). As shown in Fig. 5E–H, NE treatment increased TNF-α and IL-6 levels, decreased adiponectin levels, and increased leptin levels compared with the control group ($p < 0.05$). SB203580 partially reversed these changes, although its effect was limited. Bay 11-7082 produced a more pronounced inhibitory effect, suggesting that NF-κB plays a major role in the NE-induced inflammatory response ($p < 0.05$). As shown in Fig. 5I,J, the CCK-8 and LDH assay results showed that NE treatment significantly reduced cell viability and increased LDH release ($p < 0.05$). Both SB203580 and Bay 11-7082 partially restored cell viability and reduced LDH release ($p < 0.05$). Among them, the NF-κB inhibitor Bay 11-7082 showed a more pronounced protective effect.

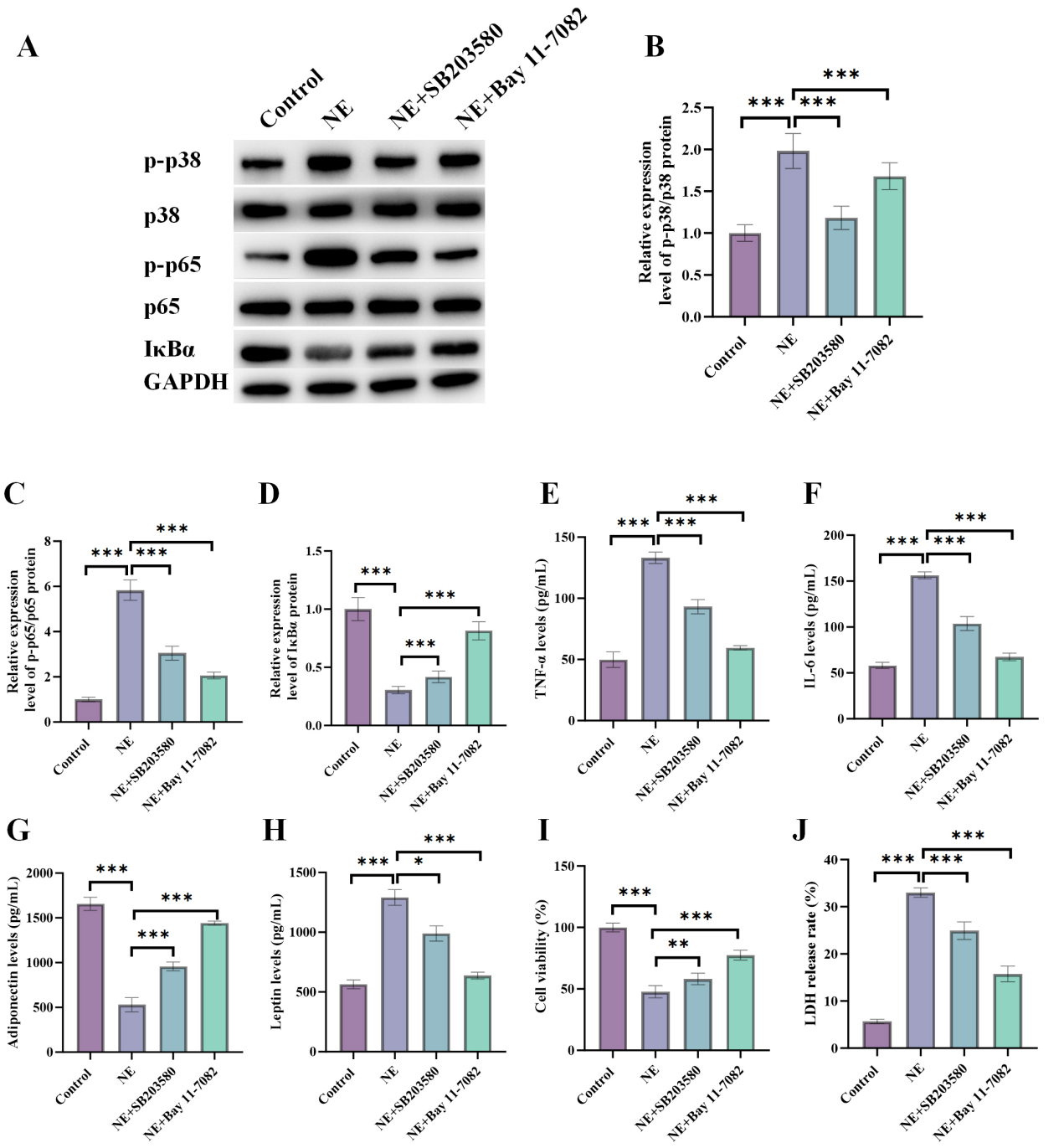


**Fig. 5. The p38 MAPK and NF-κB pathways are involved in NE-induced inflammatory responses and cellular injury in epicardial adipose-derived cells**. (A–D) Western blot analysis of p38 and NF-κB pathway activation after treatment with SB203580 and Bay 11-7082. (E–H) ELISA measurement of TNF-α, IL-6, adiponectin, and leptin levels. (I) CCK-8 assay to assess cell viability. (J) LDH release assay to evaluate cellular injury. n = 6. *$p < 0.05$, **$p < 0.01$, and ***$p < 0.001$.

## Discussion

This study showed that NE induced inflammatory, apoptotic, and cell-injury-related changes in epicardial adipose-derived cells. H9c2 cells exposed to culture supernatants collected from drug-treated epicardial adipose-derived cell cultures showed changes in Fluo-4 fluorescence intensity, calcium-handling protein and Cx43 expression, and apoptosis. Because these supernatants may have contained intracellular components released from injured cells in addition to actively released factors, the specific components responsible for the H9c2 cell responses could not be determined.

Previous studies have shown that, due to its unique anatomical location, epicardial adipose tissue (EAT) can directly influence the myocardium through paracrine effects and exhibits enhanced inflammation and dysregulated adipokine secretion in patients with atrial fibrillation [7,16]. NE treatment was associated with higher TNF-α, IL-6, and leptin levels and lower adiponectin levels in culture supernatants from epicardial adipose-derived cells. However, because NE also reduced cell viability and increased cellular injury, these extracellular changes may reflect the combined effects of inflammation-related responses, changes in the number of viable cells, and the release of intracellular components from injured cells, and therefore cannot be interpreted solely as alterations in active cellular secretion. NE also reduced lipid droplet accumulation and promoted apoptosis and autophagy-related changes. These results suggest that NE treatment exerts multiple effects on epicardial adipose-derived cells, including alterations in lipid accumulation, cell viability, apoptosis, and autophagy-related protein expression. Because autophagic flux was not assessed, the observed changes in LC3-II/LC3-I and p62 should not be interpreted as direct evidence of increased autophagic activity.

Atropine treatment alone produced modest changes in inflammatory mediators, whereas the combined treatment group showed the most pronounced changes in inflammatory indicators and pathway activation. Because no cholinergic agonist treatment or muscarinic receptor expression analysis was performed, the atropine experiment should be regarded as an exploratory pharmacological intervention rather than a model of parasympathetic inhibition or autonomic imbalance [17,18]. In addition, although the cells were washed before conditioned-medium collection, a direct contribution of residual atropine to the H9c2 cell responses cannot be completely excluded. Therefore, the effects observed in the NE + atropine-CM group cannot be attributed entirely to changes mediated by epicardial adipose-derived cells.

At the molecular level, this study confirmed that NE significantly activates the p38 MAPK and NF-κB pathways, as evidenced by increased phosphorylation of p38 and p65, IκBα degradation, and nuclear translocation of p65. Treatment with SB203580 partially attenuated the inflammatory response, whereas Bay 11-7082 exerted a more pronounced effect. However, because downstream p38 substrates were not examined, inhibition of p38 kinase activity could not be directly verified. These findings are consistent with previous studies indicating crosstalk between the MAPK and NF-κB signaling pathways [19,20,21].

A key finding of this study was that H9c2 cells exposed to culture supernatants from NE-treated epicardial adipose-derived cell cultures showed changes in calcium-related indicators. Specifically, these cells exhibited higher Fluo-4 fluorescence intensity, lower SERCA2a expression and PLB phosphorylation, higher RyR2 phosphorylation, and lower Cx43 expression. These findings indicate increased Fluo-4 fluorescence intensity and altered calcium-handling protein expression in H9c2 cells. However, calcium transient kinetics, sarcoplasmic reticulum $Ca^{2+}$ uptake and leakage, action potentials, and intercellular electrical conduction were not directly measured. Therefore, the observed changes should not be interpreted as direct evidence of impaired calcium cycling, electrical coupling, or arrhythmogenic activity.

H9c2 cells exposed to culture supernatants from differently treated epicardial adipose-derived cell cultures also showed increased apoptosis, with the highest apoptosis rate observed in the NE + atropine-CM group. Together, these results support an *in vitro* association between changes observed in epicardial adipose-derived cell cultures and calcium-related alterations and cellular injury in H9c2 cells.

This study has several limitations. First, the findings were based on *in vitro* models and require further validation in animal and clinical studies. In addition, H9c2 cells are rat cardiomyoblasts rather than mature atrial cardiomyocytes, and electrophysiological function was not directly assessed. Second, although inhibition of the p38 MAPK and NF-κB pathways attenuated NE-induced inflammatory responses and cellular injury in epicardial adipose-derived cells, conditioned media from inhibitor-treated cells were not subsequently applied to H9c2 cells. Thus, the proposed mechanistic cascade linking p38 MAPK/NF-κB-mediated changes in epicardial adipose-derived cells to H9c2 cell injury was not directly validated. Third, cells obtained from the same rat were subjected to different treatment conditions, and observations across treatment groups may therefore have been correlated within the same donor. The current statistical analyses did not explicitly account for this within-donor correlation, which represents a statistical limitation of the study. Fourth, the conditioned-media experiments also have several limitations. Although the cells were washed after drug treatment and conditioned medium was collected during a subsequent 24-h serum-free period, the samples were not normalized to the number of viable donor cells, and LDH release was not measured in the same supernatant samples used for H9c2 cell treatment. Equalizing total protein concentrations could not distinguish actively released factors from intracellular components released by injured or dying cells. Moreover, the inflammatory cytokines and adipokines measured by ELISA were not specifically quantified in the same conditioned-medium samples used for H9c2 cell treatment. Accordingly, changes in individual factors, including TNF-α, IL-6, adiponectin, and leptin, cannot be directly linked to the observed H9c2 cellular phenotype. The marked cytotoxicity observed after 10 μM NE treatment may further affect the interpretation of extracellular inflammatory mediators and adipokines because their measured levels may also be influenced by reduced cell viability and the release of intracellular components. Therefore, the specific components responsible for the ob-

served H9c2 cell responses remain uncertain. Other potential mechanisms, including oxidative stress and mitochondrial dysfunction, also warrant further investigation.

## Conclusions

In conclusion, norepinephrine activated the p38 MAPK and NF-κB signaling pathways, inducing inflammatory changes and cellular injury in epicardial adipose-derived cells. H9c2 cells exposed to culture supernatants from drug-treated epicardial adipose-derived cell cultures showed increased Fluo-4 fluorescence intensity, altered calcium-handling protein and Cx43 expression, and increased apoptosis. H9c2 cells exposed to media collected from drug-treated epicardial adipose-derived cell cultures showed calcium-related alterations and cellular injury, although the specific factors responsible for these changes remain unclear.

## Availability of Data and Materials

The data that support the findings of this study are available from the corresponding author upon reasonable request.

## Author Contributions

FL, PC, LNM, YW and SJX designed the research study. SJX performed the research. FL and SJX provided help and advice on the experiments. SJX analyzed the data. FL was responsible for writing the original draft of the manuscript. All authors contributed to important editorial changes in the manuscript. All authors read and approved the final manuscript. All authors have participated sufficiently in the work and agreed to be accountable for all aspects of the work.

## Ethics Approval and Consent to Participate

This study has been approved by the Ethics Committee of the People's Hospital of Ningxia Hui Autonomous Region (Approval No. 2026-LL-228). All procedures complied with the ARRIVE guidelines 2.0.

## Acknowledgment

Not applicable.

## Funding

This research received no external funding.

## Conflict of Interest

The authors declare no conflict of interest.

## References

[1] Saleh K, Haldar S. Atrial fibrillation: a contemporary update. Clinical Medicine (London, England). 2023; 23: 437–441. https://doi.org/10.7861/clinmed.2023-23.5.Cardio2

[2] Conte M, Petraglia L, Cabaro S, Valerio V, Poggio P, Pilato E, et al. Epicardial Adipose Tissue and Cardiac Arrhythmias: Focus on Atrial Fibrillation. Frontiers in Cardiovascular Medicine. 2022; 9: 932262. https://doi.org/10.3389/fcvm.2022.932262

[3] Takahashi N, Abe I, Kira S, Ishii Y. Role of epicardial adipose tissue in human atrial fibrillation. Journal of Arrhythmia. 2023; 39: 93–110. https://doi.org/10.1002/joa3.12825

[4] Shaihov-Teper O, Ram E, Ballan N, Brzezinski RY, Naftali-Shani N, Masoud R, et al. Extracellular Vesicles From Epicardial Fat Facilitate Atrial Fibrillation. Circulation. 2021; 143: 2475–2493. https://doi.org/10.1161/CIRCULATIONAHA.120.052009

[5] Ding Y, Lin F, Liu Z, Zhou X, Liang X. Targeting Epicardial/Pericardial Adipose Tissue in Cardiovascular Diseases: A Novel Therapeutic Strategy. Reviews in Cardiovascular Medicine. 2025; 26: 26128. https://doi.org/10.31083/RCM26128

[6] Si Y, Feng Z, Liu Y, Fan W, Shan W, Zhang Y, et al. Inflammatory biomarkers, angiogenesis and lymphangiogenesis in epicardial adipose tissue correlate with coronary artery disease. Scientific Reports. 2023; 13: 2831. https://doi.org/10.1038/s41598-023-30035-x

[7] Li J, Zhao M, Bai L, Zhao J, Gao H, Bai M. Recent Advances in Inflammation-Associated Epicardial Adipose Tissue for Atrial Fibrillation Patients. Reviews in Cardiovascular Medicine. 2025; 26: 36598. https://doi.org/10.31083/RCM36598

[8] Hu Z, Ding L, Yao Y. Atrial fibrillation: mechanism and clinical management. Chinese Medical Journal. 2023; 136: 2668–2676. https://doi.org/10.1097/CM9.0000000000002906

[9] Jin H, Ding L, Li B, Zhang J. Data Analysis of Heart Rate Variability and Arrhythmia in Patients with Paroxysmal Atrial Fibrillation. Discovery Medicine. 2024; 36: 1610–1615. https://doi.org/10.24976/Discov.Med.202436187.147

[10] Carbone AM, Del Calvo G, Nagliya D, Sharma K, Lymperopoulos A. Autonomic Nervous System Regulation of Epicardial Adipose Tissue: Potential Roles for Regulator of G Protein Signaling-4. Current Issues in Molecular Biology. 2022; 44: 6093–6103. https://doi.org/10.3390/cimb44120415

[11] Nigdelioglu Dolanbay S, Şirin S, Aslim B. Allocryptopine Attenuates Inflammatory Responses in Microglial Cells Via TLR4-Dependent NF-κB and p38 MAPK Pathways. Molecular Neurobiology. 2025; 62: 3833–3847. https://doi.org/10.1007/s12035-024-04520-x

[12] Nagoor Meeran MF, Arunachalam S, Azimullah S, Saraswathiamma D, Albawardi A, Almarzooqi S, et al. α-Bisabolol, a Dietary Sesquiterpene, Attenuates Doxorubicin-Induced Acute Cardiotoxicity in Rats by Inhibiting Cellular Signaling Pathways, Nrf2/Keap-1/HO-1, Akt/mTOR/GSK-3β, NF-κB/p38/MAPK, and NLRP3 Inflammasomes Regulating Oxidative Stress and Inflammatory Cascades. International Journal of Molecular Sciences. 2023; 24: 14013. https://doi.org/10.3390/ijms241814013

[13] Ren AJ, Wei C, Liu YJ, Liu M, Wang P, Fan J, et al. ZBTB20 Regulates SERCA2a Activity and Myocardial Contractility Through Phospholamban. Circulation Research. 2024; 134: 252–265. https://doi.org/10.1161/CIRCRESAHA.123.323798

[14] Ye B, Zhou H, Chen Y, Luo W, Lin W, Zhao Y, et al. USP25 Ameliorates Pathological Cardiac Hypertrophy by Stabilizing SERCA2a in Cardiomyocytes. Circulation Research. 2023; 132: 465–480. https://doi.org/10.1161/CIRCRESAHA.122.321849

[15] Lamounier-Zepter V, Look C, Alvarez J, Christ T, Ravens U, Schunck WH, et al. Adipocyte fatty acid-binding protein suppresses cardiomyocyte contraction: a new link between obesity and heart disease. Circulation Research. 2009; 105: 326–334. https://doi.org/10.1161/CIRCRESAHA.109.200501

[16] Patel KHK, Hwang T, Se Liebers C, Ng FS. Epicardial adipose tissue as a mediator of cardiac arrhythmias. American Journal of Physiology. Heart and Circulatory Physiology. 2022; 322: H129–H144. https://doi.org/10.1152/ajpheart.00565.2021

[17] Mikhailov A, Arora R, Pfenniger A. Autonomic dysregulation and atrial arrhythmias. American Journal of Physiology. Cell Physiology. 2025; 329: C1439–C1450. https://doi.org/10.1152/ajpcell.00537.2025

[18] Vandenberk B, Haemers P, Morillo C. The autonomic nervous system in atrial fibrillation-pathophysiology and non-invasive assessment. Frontiers in Cardiovascular Medicine. 2024; 10: 1327387. https://doi.org/10.3389/fcvm.2023.1327387

[19] Mao H, Zhao X, Sun SC. NF-κB in inflammation and cancer. Cellular & Molecular Immunology. 2025; 22: 811–839. https://doi.org/10.1038/s41423-025-01310-w

[20] Zhao H, Wu L, Yan G, Chen Y, Zhou M, Wu Y, et al. Inflammation and tumor progression: signaling pathways and targeted intervention. Signal Transduction and Targeted Therapy. 2021; 6: 263. https://doi.org/10.1038/s41392-021-00658-5

[21] Zhang Y, Ding J, Wang Y, Feng X, Du M, Liu P. Guanxinkang Decoction Attenuates the Inflammation in Atherosclerosis by Regulating Efferocytosis and MAPKs Signaling Pathway in LDLR$^{-/-}$ Mice and RAW264.7 Cells. Frontiers in Pharmacology. 2021; 12: 731769. https://doi.org/10.3389/fphar.2021.731769